Published in final edited form as:
Int J Radiat Oncol Biol Phys. 2008 September 1; 72(1): 236–246. doi:10.1016/j.ijrobp.2008.04.051.

Intrafractional Motion of the Prostate During Hypofractionated Radiotherapy

Yaoqin Xie, Ph.D.[*], **David Djajaputra, Ph.D.**[*], **Christopher R. King, Ph.D., M.D.**[*], **Sabbir Hossain, Ph.D.**[†], **Lijun Ma, Ph.D.**[†], and **Lei Xing, Ph.D.**[*,a)]

[*]Department of Radiation Oncology, Stanford University School of Medicine, Stanford, CA

[†]Department of Radiation Oncology, University of California San Francisco, San Francisco, CA

Abstract

Purpose—To report the characteristics of prostate motion as tracked by the stereoscopic X-ray images of the implanted fiducials during hypofractionated radiotherapy with CyberKnife.

Methods and Materials—Twenty one patients with prostate cancer who were treated with CyberKnife between January 2005 and September 2007 were selected for this retrospective study. The CyberKnife uses a stereoscopic X-ray system to obtain the position of the prostate target through the monitoring of implanted gold fiducial markers. If there is a significant deviation, the treatment is paused while the patient is repositioned by moving the couch. The deviations calculated from X-ray images acquired within the time interval between two consecutive couch motions constitute a data set.

Results—A total of 427 data sets and 4439 time stamps of X-ray images were analyzed. The mean duration for each data set is 697 s. At 30 s, a motion larger than 2 mm exists in about 5% of data sets. The percentage is increased to 8%, 11%, and 14% at 60 s, 90 s, and 120 s, respectively. A similar trend exists for other values of prostate motion.

Conclusions—With proper monitoring and intervention during treatment, the prostate shifts observed among the patients can be kept within the tracking range of the CyberKnife. On average a sampling rate of ~40 s between consecutive X-rays is acceptable to ensure sub-millimeter tracking. However, there is significant movement variation among patients and higher sampling rate may be necessary in some patients.

Keywords

CyberKnife; Prostate cancer; Fiducial markers; Real-time tracking

INTRODUCTION

Recent randomized studies for patients with localized prostate cancer confirm that improved biochemical failure-free survival was achieved by using higher doses of external beam

a)Author to whom correspondence should be addressed. Stanford University School of Medicine, Department of Radiation Oncology, 875 Blake Wilbur Drive, Stanford, CA 94305-5847, E-mail: lei@reyes.stanford.edu, Phone: (650)498-7896, Fax: (650)498-4015.

Conflicts of Interest Notification: No actual or potential conflicts of interest exist.

radiotherapy (RT) (1–3). Although higher dose is good for tumor control, it also carries higher risk of complications to surrounding critical structures, such as the bladder and rectum (4). Because of the inter- and intra-fractional motion of the prostate margin is required when planning a prostate radiotherapy. Knowing the extent of prostate movement during a fractionated, and more importantly a hypofractionated, treatment is necessary to reduce the treatment margin and facilitate prostate dose escalation (5,6). A number of techniques have been developed for measuring setup variations and internal organ motions for individual patients from day-to-day and during a treatment fraction (7).

Ultrasound has been a useful tool for prostate target localization (8–10). Fung et al. (8) analyzed the data of 7825 daily fractions of 234 prostate patients and indicated average 3D inter-fractional displacement of about 7.8 mm. EPID and/or on-board kV X-ray imaging of implanted fiducials is also widely used for initial setup and interfractional monitoring of the prostate target position (11–17). A recent development in measuring setup variations is the electromagnetic positioning and continuous monitoring system from Calypso Medical Technologies (Seattle, WA) (18–20). The difference between skin marks vs. the Calypso System alignment was found to be greater than 5 mm in vector length in more than 75% of fractions. Displacements greater than 3 mm and 5 mm for cumulative durations of at least 30 s were observed during 41% and 15% of sessions, respectively.

At our institution, CyberKnife (Accuray, Inc.) has been employed for a phase II hypofractionated treatment of prostate cancer. By frequent stereoscopic X-ray imaging of implanted fiducials, the CyberKnife provides an effective way to monitor the position of the prostate target during a hypofractionated treatment (21). The system records the center of mass (CM) of implanted fiducials as computed from each pair of stereoscopic images during each treatment, thus providing a valuable set of data to better understand the intra-fractional movement of the prostate. In addition to the technical difference in monitoring the implanted fiducials, a major feature of our data is that the time span of tumor motion monitoring is significantly longer as compared to the Calypso data (up to 2500 s with a mean duration of about 700 s vs. 600 s for Calypso). This study sheds useful insight into features of intra-fractional prostate motion and re-emphasizes the need for an effective means of compensating the intra-fractional prostate movement to ensure adequate dose coverage of the tumor target.

METHODS AND MATERIALS

CyberKnife data acquisition

During hypofractionated prostate radiation treatment, fiducials must be rigidly fixed no more than 5–6 cm relative to a known reference or relative to the tumor. Any fiducial migration will degrade the accuracy of fiducial based targeting. Commonly, three fiducials are used for prostate cancer treatment.

The patient setup and treatment delivery process is illustrated in Fig. 1. First, orthogonal X-ray images are acquired before treatment. The system determines the absolute position of the target volume via image-to-DRR (digitally reconstructed radiograph) registration. The three-dimensional translation and rotation deviation of the target from the planned position is calculated. The deviation is corrected by manually moving the treatment couch. The treatment starts if the computed shift is less than a pre-set threshold, 1 cm in general. During treatment, the robot automatically adjusts the incident beam to compensate for the target deviation. The CyberKnife system can perform up to 10 mm translational correction. However, the larger the deviation, the greater is the uncertainty in the accuracy of the robot correction. Therefore it is recommended that the deviation during treatment be kept to minimum. At Stanford a threshold of ~5 mm translation is normally used. During the beam delivery X-ray images are acquired every 3 nodes, which amounts to about 40 s interval. The shift of X-ray images from the

planning CT is monitored in real-time. If the calculated shift is more than the given threshold, the treatment will be paused and the manual couch movement is required until the shift is below the limit.

Patient selection and prostate motion data analysis

The patients were treated with hypofractionated protocol consisting of five fractions of 7.25 Gy per fraction delivered every other day. In total 21 prostate cancer patients were treated under the protocol between Jan. 2005 and Sep. 2007 for the study. In our analysis, one fraction can generate more than one data set because the treatment is usually paused a few times to reposition the patient by couch movement. The couch displacement is not kept in treatment log-file, therefore the data sets before and after the intervening couch movement cannot be joined together without manually writing down the couch shifts during the treatment process.

After patient treatment, a log-file containing the CM displacements of the fiducials in anterior/posterior (AP), left/right (LR), and superior/inferior (SI) directions is saved in the CyberKnife control computer and can be readily used for the analysis of prostate movement during the beam delivery process. In addition, files containing the Rigid Body Error (RBE) data of each implanted fiducial are recorded at each time stamp in the Accuray CyberKnife System. The RBE at a time stamp is defined as the distance of fiducial from its corresponding CT position after the system figures out the best translation and rotation transformation by a rigid registration of the projection images and the CT-generated DRRs. For the 21 patients studied here, we first analyzed the statistical characteristics of the collected time duration data sets. This analysis provides valuable information on the average time it takes for the prostate to reach the pre-set threshold. The CM displacement log-files acquired during the treatment course were then studied and the overall and the patient specific behaviors of the prostate displacement were investigated.

Study of prostate deformation

The RBE values mentioned above were employed to gain an understanding of prostate deformation. In general, the intra-fractional motion of prostate consists of rigid and deformable motions. The rigid motion of prostate is characterized by the CM displacement of the three implanted fiducials and any potential rotation. In principle, it is possible to estimate the prostate rotation based on the angular change of the fiducial configuration. But the prostate rotation is generally small and negligible. We have therefore focused our study on translation and deformable motions of the prostate. To a certain extent, the deformation can be described by the RBE values and the correlation between RBE curves of the three implanted fiducials. In an ideal case where there is no deformation, the RBE should be zero and the three time-dependent RBE curves would correlate completely. The correlation between three fiducials was computed for four representative cases.

Influence of X-ray image sampling rate

A clinically important question in stereoscopic image guided prostate treatment is the optimal X-ray imaging frequency. Here the optimal imaging frequency is defined as the frequency which minimizes the patient exposure while not missing any significant movement of the target during the beam-off interval of the imaging X-ray (22). To better understand the issue, we investigated the consequence of down-sampling the X-ray imaging data for one of the patients.

RESULTS

Duration of data sets

For the 21 patients, a total of 4439 time stamps, which constitute 427 separate data sets, were recorded. Figure 2 shows the histogram of the duration of the 427 data sets. The bin size is 200 s and the mean duration is 697 s. The duration of a data set represents the time for the prostate to move beyond an acceptable level to the therapist (~5 mm shift for prostate at our institution). Thus, a shorter duration corresponds to a more prominent prostate movement. The data here suggest that on average it takes 697 s for the prostate to move beyond 5 mm relative to its planned position.

Overall behavior of intra-fractional prostate motion

A useful way to present the prostate motion data is to show the histogram of the fiducial CM movement in different directions. As seen in Fig. 3 the prostate is more stable in the LR direction, which is consistent with pelvic and prostate anatomy. Generally, the shift distribution in SI direction is similar to that in AP direction. The mean shift in each direction, averaged over all patients, was 1.55 ± 1.28 mm, 0.87 ± 1.17 mm, 1.80 ± 1.44 mm in SI, LR, and AP directions, respectively. The average vector length of the shift is 2.61 ± 1.94 mm. Table 1 summarizes the statistical characterization of the data for each direction and the vector length of the shift. It should be emphasized that these mean values were specific to the 5 mm threshold used in fiducial tracking because the greater-than-threshold shifts were reset by manual couch adjustments. It therefore does not represent the mean magnitude of prostate motion during a complete treatment fraction.

An alternative way to present the data of Fig. 3 is to illustrate the histogram of the prostate movement as a function of time duration and shift as shown in Fig. 4. Each color represents a specific time segment. It is clear that as the time elapses, the spatial distribution of the prostate becomes increasingly spread out. From these plots, it is also clear that SI and AP movements are similar, whereas the LR curve is more concentrative.

A rolling average (23) of total movement distance was computed in equal time interval stamp to further illustrate the prostate movement tendency as shown in Fig. 5. Since the average image acquisition interval is ~40 s and using the Nyquist sampling theory (24), a time interval of 20 s is used to calculate the rolling average curve. The rolling average window was set to be 120 s. Thus, the average shift at 0 s is a result of shifts from 0 s to 60 s, and the average shift at 100 s represents the contributions from 40 s to 160 s. Since there are not enough data for rolling average calculation at the end of the time duration, the calculation stopped at 1400 s in Fig. 5. The curve in Fig. 5 represents a logarithmic fit of the data. It can be seen that the prostate movement increases against time.

Patient specific behavior of intra-fractional prostate motion

The motion of the CM of the three implanted fiducials is used as a surrogate of prostate motion. This quantity was recorded over time and analyzed for the 427 data sets (on average 20 data sets per patient). For illustration, a selection of six typical patterns of motion categories is shown in Fig. 6(a–f). The *x*-axis represents the time stamp, and the *y*-axis is the motion shift. Similar to those observed by Kupelian et al (18), these patterns vary from stable positioning at baseline (Fig. 6a), continuous drift (Fig. 6b), transient excursion (Fig. 6c), persistent excursion (Fig. 6d), and high-frequency excursion (Fig. 6e). Some patterns are simply too irregular to categorize into any of the above classes (Fig. 6f).

It should be noted that, for each patient the prostate movement pattern may change from fraction to fraction or even from data set to data set within the same treatment fraction. Figure 7 shows

the prostate movement behavior for one of the patients. This patient received five treatment fractions and each fraction contains two data sets. Data sets 2, 4, 5 are the continuous drift; data set 3 is the transient excursion; data sets 1, 7, 8 consist of two continuous drifts; data sets 6 and 9 are high-frequency excursions followed by a stable positioning at baseline; and data set 10 shows a continuous drift followed by a stable positioning at baseline. These data suggest that the prostate intra-fractional motion is somewhat random and does not follow a fixed pattern.

Influence of prostate deformation

Prostate deformation is of a practical concern. In Fig. 8 the RBE curves for each fiducial are plotted for four representative patients. The RBE value is generally within 1.5 mm, indicating that the deformation of prostate is not a major issue here. Furthermore, as listed in Table 2, the correlation coefficients between RBE curves of the three implanted fiducials were found to be close to 100%. Although the fiducial movement profiles are different for different patients, the motion behaviors of 3 fiducials for each patient are similar, indicating that no prominent deformation occurred in these cases.

Optimal image sampling rate

To understand the influence of X-ray image sampling rate, we extracted a fraction of movement from one of the patients as shown in the solid line of Fig. 9(a). Now suppose that the images are acquired at every other time stamp in the original acquisition schedule, the prostate movement curve would look quite different, as indicated in the dashed one of Fig. 9(a). Figure 9(b) is another example of CM movement curve captured by two different sampling rates. The peak in the solid curve revealed by a higher sampling rate disappears when the sampling rate is reduced. It is difficult to guarantee that there is no peak value in a relatively long sample interval. However, more frequent real-time imaging, which provides more accurate correction to the treatment robot, would result in longer treatment time and the increase of patient's normal-tissue dose.

In reality, a few factors may influence the selection of the sampling rate of the X-ray imaging, which include the dose rate, patient specific characteristics, the fractionation scheme, etc. Therefore a tradeoff between imaging frequency and target position accuracy needs to be made. A rule of thumb is that the movement of prostate within the interval of two consecutive images should be less than a pre-specified criterion, say 1 or 2 mm. Due to the randomness of the prostate movement, this decision can only be made based on a statistical basis. The sampling rate should be chosen in such a way that the number of data sets with displacement exceeding a pre-specified motion range should be statistically small. Figure 10 shows a plot of the percentage for the prostate target to move more than 1 mm, 2 mm, 3 mm, 4 mm, 5 mm, …, at 30 s, 60 s, 90 s, 120 s…. This figure is useful in helping us to find out the suitable sampling rate for a pre-specified prostate motion range. For example, if a motion larger than 2 mm is permissible for less than 5% of the data sets (in other words, if it is desired to keep 95% of the data sets to have a motion less than 2 mm), from Fig. 10, it is seen that a 30 s sampling duration should be used. If a 60 s duration is used, 7.5% of the data sets will have a motion larger than 2 mm. For 90 s and 120 s durations, the percentage having motion greater than 2 mm will be increased to 11% and 14%, respectively. For convenience, the percentage of data sets having motion greater than 1 mm to 5 mm is summarized in Table 3 for a few sampling intervals of interest.

DISCUSSION

To cope with the uncertainty in patient setup and tumor target localization a commonly used method is to add a population based safety margin to the target and sensitive structures to ensure

adequate dose coverage of the target given the uncertainty, which significantly compromises the success of radiation therapy (25). Because of the proximity of the prostate to the rectum and bladder, a robust strategy in locating the tumor target is necessary if the radiation dose to the prostate is to be escalated in order to substantially enhance the probability of curing patients without damaging the sensitive structures. A detailed knowledge of prostate motion would help to understand the nature and degree of the adverse influence of the uncertainty and provide guidance in dealing with the issue. The known motion patterns can also be included into inverse planning process as to minimize its adverse dosimetric influence.

It is important to bear in mind that the proposed method relies on the assumption that the markers accurately reflect the position of the prostate. In other words, the implanted markers do not migrate significantly within the prostate during the course of treatment. Pouliot et al. studied the issue by analyzing the orthogonal portal images of 11 patients (26). The distances between three markers were determined and monitored over the course of therapy to assess the magnitude of marker migration. The average standard deviation (SD) of the distances was found to be 1.3 mm. Similar observation has been made by Poggi et al (27), Nichol et al (1), and Shirato et al (28).

The prostate deformation study presented here is estimation in nature, primarily because the RBE and the correlation between RBE curves of fiducials for each patient are less quantitative in assessing the organ deformation. However, it is useful quantity and sheds practical insight into the problem. A more thorough study based on biomechanical measures of the prostate deformation as a function of time is highly desirable to completely understand the issue.

There are several drawbacks associated with fiducial-based image-guided prostate radiation therapy. Other than the fact that it involves an invasive procedure of fiducial implantation, the fiducial tracking used in CyberKnife or Calypso system is limited to “rigid” tumors. While our data indicated that the deformation of the prostate gland during the hypofractionated treatment is small and the CM of the three implanted fiducials can be used to describe the prostate position, it is important to remind that locating the prostate is only part of the overall task in prostate radiation therapy. In reality, tracking the motion of various involved sensitive structures represents the other side of the “coin” and is also of critical importance to the success of IGRT. Therefore, knowing the spatial location and geometric shapes of the sensitive structures is also critical to customize the dose distribution to maximize the dose to the target while sparing the adjacent sensitive structures. On a fundamental level, the motion of prostate target is often caused by the motion or physiological change of the sensitive structures.

This study and most if not all studies have focused on prostate-only treatment. Clinically, the treatment of intermediate- and high-risk prostate cancer often involves the irradiation of seminal vesicles and regional lymph nodes. The implanted fiducials in these cases are less helpful in locating the seminal vesicles and pelvic nodes. A better imaging method capable of providing 3D anatomy would be highly desirable. On-board cone beam CT (CBCT) has recently become available to provide volumetric information of a patient in the treatment position (29), and holds promises for improved target localization and irradiation dose verification (30). CBCT is valuable in providing 3D or even 4D patient model before treatment and affords a useful solution to reduce the adverse effect of inter-fraction organ motion (22, 31–34). However, acquiring real-time patient geometric information during radiation delivery using an on-board imaging device is still impractical. A combined use of pre-treatment patient geometric model derived from 3D/4D CBCT and real-time stereoscopic X-ray projection data may be useful to estimate the location of target and adjacent sensitive structures. This investigation is still in progress and will be reported in the future.

CONCLUSION

Intra-fractional organ motion has long been recognized as one of the major limiting factors of prostate dose escalation in conformal radiation therapy. A detailed knowledge of prostate motion would help to understand the nature and degree of the adverse influence of the uncertainty and provide guidance in dealing with the issue. The known motion patterns can also be included into inverse planning process as to minimize its adverse dosimetric influence. Our study shows the importance of real-time image guidance and motion-compensation technique such as the robotic linear accelerator used in CyberKnife during hypofractionated prostate radiation treatment. Given the magnitude and random nature of prostate motion as well as the recent technical advancements in various related fields, real-time monitoring of prostate position to adaptively compensate the motion should be part of future prostate radiation therapy to ensure adequate dose coverage of the prostate target while maintaining an adequate sparing of the sensitive structures.

ACKNOWLEDGEMENT

This work was supported in part by grants from the Department of Defense (PC040282) and National Cancer Institute (1R01 CA98523 and CA104205).

REFERENCES

1. Nichol AM, Brock KK, Lockwood GA, et al. A magnetic resonance imaging study of prostate deformation relative to implanted gold fiducial markers. Int J Radiat Oncol Biol Phys 2007;67:48–56. [PubMed: 17084546]
2. Zietman AL, DeSilvio ML, Slater JD, et al. Comparison of conventional-dose vs high-dose conformal radiation therapy in clinically localized adenocarcinoma of the prostate: a randomized controlled trial. Jama 2005;294:1233–1239. [PubMed: 16160131]
3. Pollack A, Zagars GK, Starkschall G, et al. Prostate cancer radiation dose response: results of the M. D. Anderson phase III randomized trial. Int J Radiat Oncol Biol Phys 2002;53:1097–1105. [PubMed: 12128107]
4. King CR, Lehmann J, Adler JR, et al. CyberKnife radiotherapy for localized prostate cancer: rationale and technical feasibility. Technol Cancer Res Treat 2003;2:25–30. [PubMed: 12625751]
5. Van den Heuvel F, Powell T, Seppi E, et al. Independent verification of ultrasound based image-guided radiation treatment, using electronic portal imaging and implanted gold markers. Med Phys 2003;30:2878–2887. [PubMed: 14655934]
6. Chen J, Lee RJ, Handrahan D, et al. Intensity-modulated radiotherapy using implanted fiducial markers with daily portal imaging: assessment of prostate organ motion. Int J Radiat Oncol Biol Phys 2007;68:912–919. [PubMed: 17459605]
7. Langen KM, Jones DT. Organ motion and its management. Int J Radiat Oncol Biol Phys 2001;50:265–278. [PubMed: 11316572]
8. Fung AY, Ayyangar KM, Djajaputra D, et al. Ultrasound-based guidance of intensity-modulated radiation therapy. Med Dosim 2006;31:20–29. [PubMed: 16551526]
9. Chandra A, Dong L, Huang E, et al. Experience of ultrasound-based daily prostate localization. Int J Radiat Oncol Biol Phys 2003;56:436–447. [PubMed: 12738318]
10. Langen KM, Pouliot J, Anezinos C, et al. Evaluation of ultrasound-based prostate localization for image-guided radiotherapy. Int J Radiat Oncol Biol Phys 2003;57:635–644. [PubMed: 14529767]
11. Langen KM, Meeks SL, Poole DO, et al. The use of megavoltage CT (MVCT) images for dose recomputations. Phys Med Biol 2005;50:4259–4276. [PubMed: 16148392]
12. Meeks SL, Harmon JF Jr, Langen KM, et al. Performance characterization of megavoltage computed tomography imaging on a helical tomotherapy unit. Med Phys 2005;32:2673–2681. [PubMed: 16193798]
13. Pouliot J, Bani-Hashemi A, Chen J, et al. Low-dose megavoltage cone-beam CT for radiation therapy. Int J Radiat Oncol Biol Phys 2005;61:552–560. [PubMed: 15736320]

14. Litzenberg DW, Balter JM, Lam KL, et al. Retrospective analysis of prostate cancer patients with implanted gold markers using off-line and adaptive therapy protocols. Int J Radiat Oncol Biol Phys 2005;63:123–133. [PubMed: 16111580]
15. Balter JM, Lam KL, McGinn CJ, et al. Improvement of CT-based treatment-planning models of abdominal targets using static exhale imaging. Int J Radiat Oncol Biol Phys 1998;41:939–943. [PubMed: 9652861]
16. Wong JR, Grimm L, Uematsu M, et al. Image-guided radiotherapy for prostate cancer by CT-linear accelerator combination: prostate movements and dosimetric considerations. Int J Radiat Oncol Biol Phys 2005;61:561–569. [PubMed: 15667979]
17. Poulsen PR, Muren LP, Hoyer M. Residual set-up errors and margins in on-line image-guided prostate localization in radiotherapy. Radiother Oncol. 2007
18. Kupelian P, Willoughby T, Mahadevan A, et al. Multi-institutional clinical experience with the Calypso System in localization and continuous, real-time monitoring of the prostate gland during external radiotherapy. Int J Radiat Oncol Biol Phys 2007;67:1088–1098. [PubMed: 17187940]
19. Balter JM, Wright JN, Newell LJ, et al. Accuracy of a wireless localization system for radiotherapy. Int J Radiat Oncol Biol Phys 2005;61:933–937. [PubMed: 15708277]
20. Willoughby TR, Kupelian PA, Pouliot J, et al. Target localization and real-time tracking using the Calypso 4D localization system in patients with localized prostate cancer. Int J Radiat Oncol Biol Phys 2006;65:528–534. [PubMed: 16690435]
21. Dieterich, S. Dynamic Tracking of Moving Tumors in Stereotactic Radiosurgery. In: Mould, RF., editor. Robotic Radiosurgery. Vol. Vol 1. 2005. p. 51-63.
22. Xing L, Thorndyke B, Schreibmann E, et al. Overview of image-guided radiation therapy. Med Dosim 2006;31:91–112. [PubMed: 16690451]
23. Riley, JD. Evaluation of travel time estimates derived from automatic vehicle identification tags. Department of Civil Engineering: Virginia Polytechnic Institute; 1999. p. 98-102.
24. Jones NB, Watson M. Digital Signal Processing: Principles, Devices, and Applications: IET. 1990
25. Rasch C, Steenbakkers R, van Herk M. Target definition in prostate, head, and neck. Semin Radiat Oncol 2005;15:136–145. [PubMed: 15983939]
26. Pouliot J, Aubin M, Langen KM, et al. (Non)-migration of radiopaque markers used for on-line localization of the prostate with an electronic portal imaging device. Int J Radiat Oncol Biol Phys 2003;56:862–866. [PubMed: 12788196]
27. Poggi MM, Gant DA, Sewchand W, et al. Marker seed migration in prostate localization. Int J Radiat Oncol Biol Phys 2003;56:1248–1251. [PubMed: 12873668]
28. Shirato H, Harada T, Harabayashi T, et al. Feasibility of insertion/implantation of 2.0-mm-diameter gold internal fiducial markers for precise setup and real-time tumor tracking in radiotherapy. Int J Radiat Oncol Biol Phys 2003;56:240–247. [PubMed: 12694845]
29. Jaffray DA, Siewerdsen JH, Wong JW, et al. Flat-panel cone-beam computed tomography for image-guided radiation therapy. Int J Radiat Oncol Biol Phys 2002;53:1337–1349. [PubMed: 12128137]
30. Yang Y, Schreibmann E, Li T, et al. Evaluation of on-board kV cone beam CT (CBCT)-based dose calculation. Phys Med Biol 2007;52:685–705. [PubMed: 17228114]
31. Li T, Koong A, Xing L. Enhanced 4D cone-beam CT with inter-phase motion model. Med Phys 2007;34:3688–3695. [PubMed: 17926972]
32. Li T, Schreibmann E, Yang Y, et al. Motion correction for improved target localization with on-board cone-beam computed tomography. Phys Med Biol 2006;51:253–267. [PubMed: 16394337]
33. Li T, Xing L. Optimizing 4D cone-beam CT acquisition protocol for external beam radiotherapy. Int J Radiat Oncol Biol Phys 2007;67:1211–1219. [PubMed: 17197125]
34. Sonke JJ, Zijp L, Remeijer P, et al. Respiratory correlated cone beam CT. Med Phys 2005;32:1176–1186. [PubMed: 15895601]

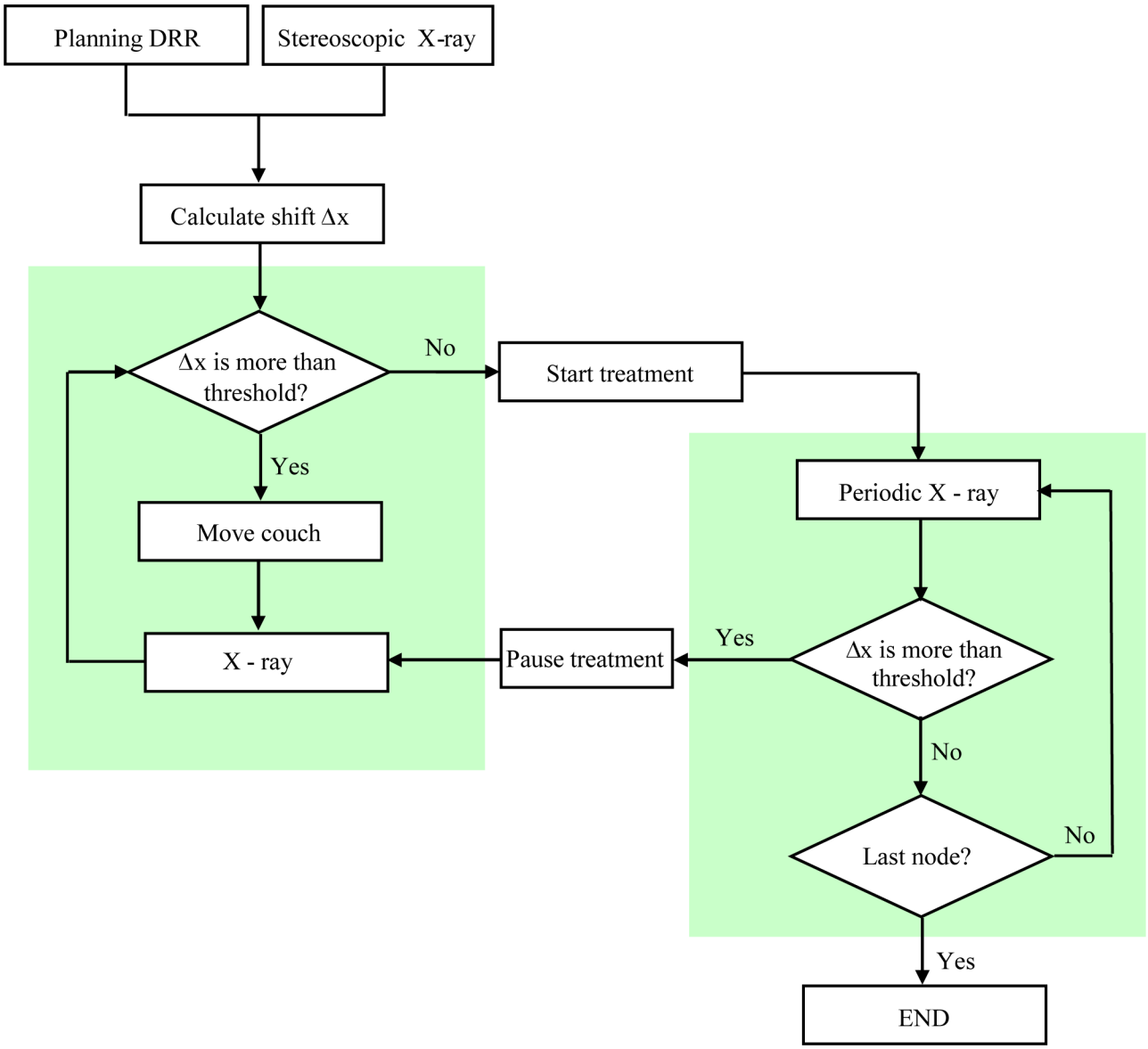

Figure 1.
Flowchart of the patient setup and delivery process in CyberKnife treatment.

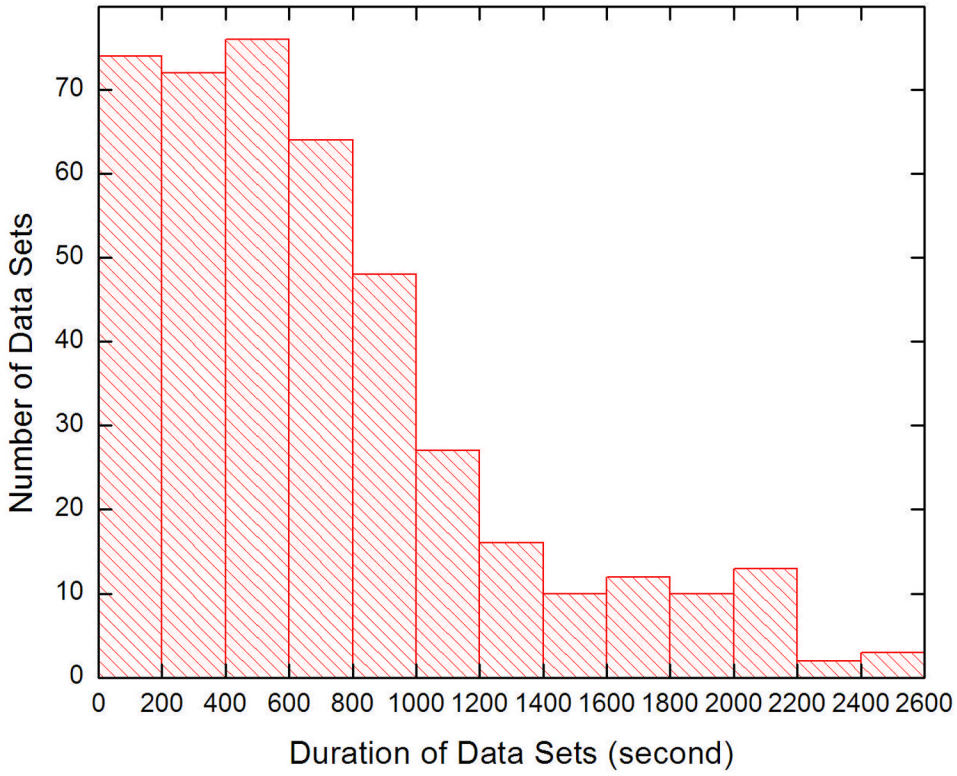

Figure 2.
Histogram of the time span of the studied data sets.

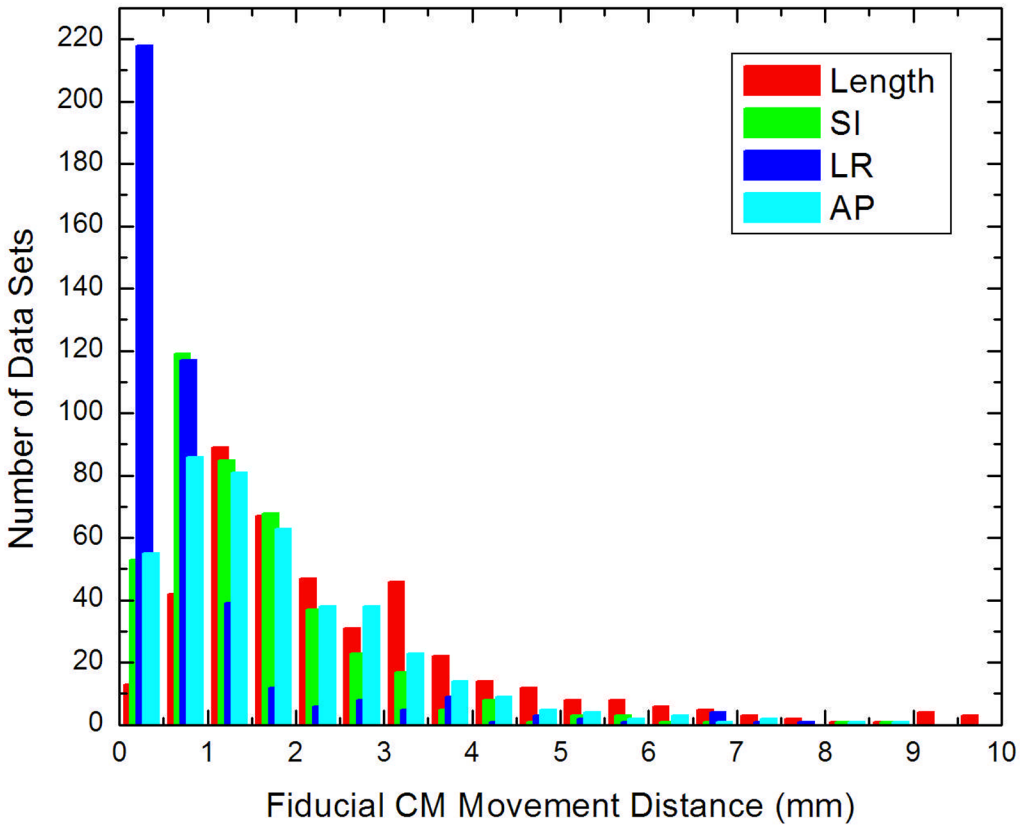

Figure 3.
Histogram of the fiducial center of mass movement in different directions.

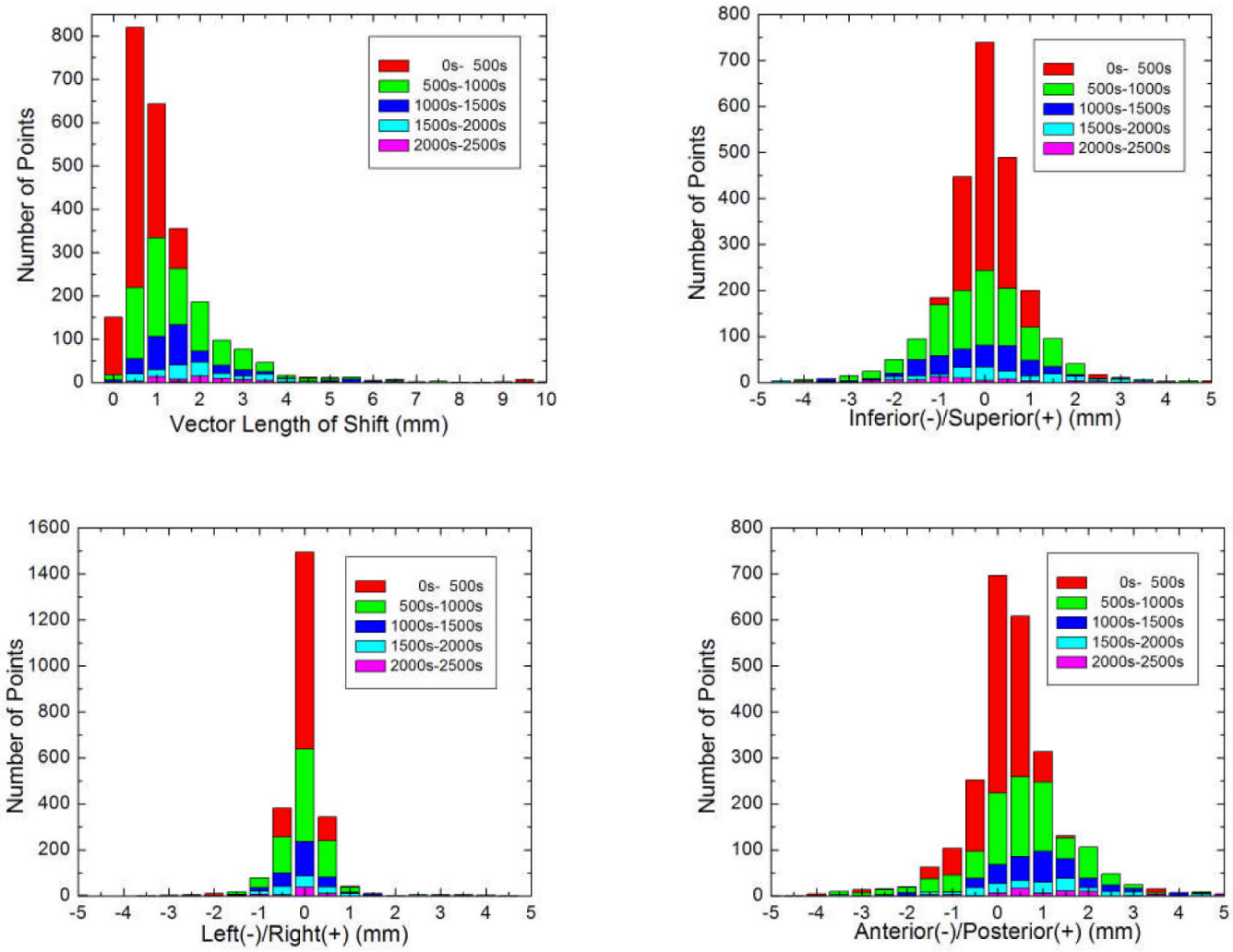

Figure 4.
Histogram of the prostate movement as a function of time duration and shift.

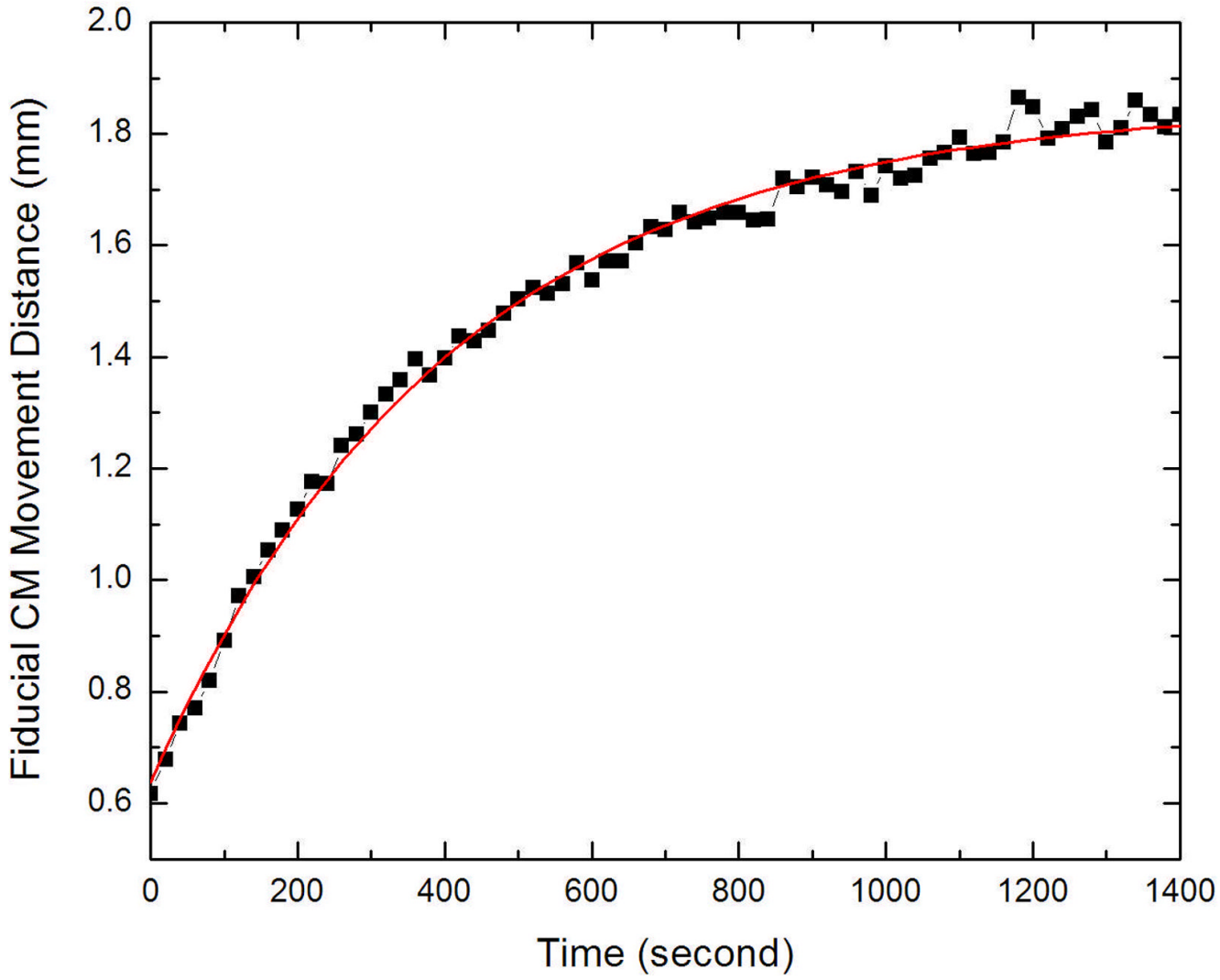

Figure 5.
Rolling averages of prostate center of mass movement.

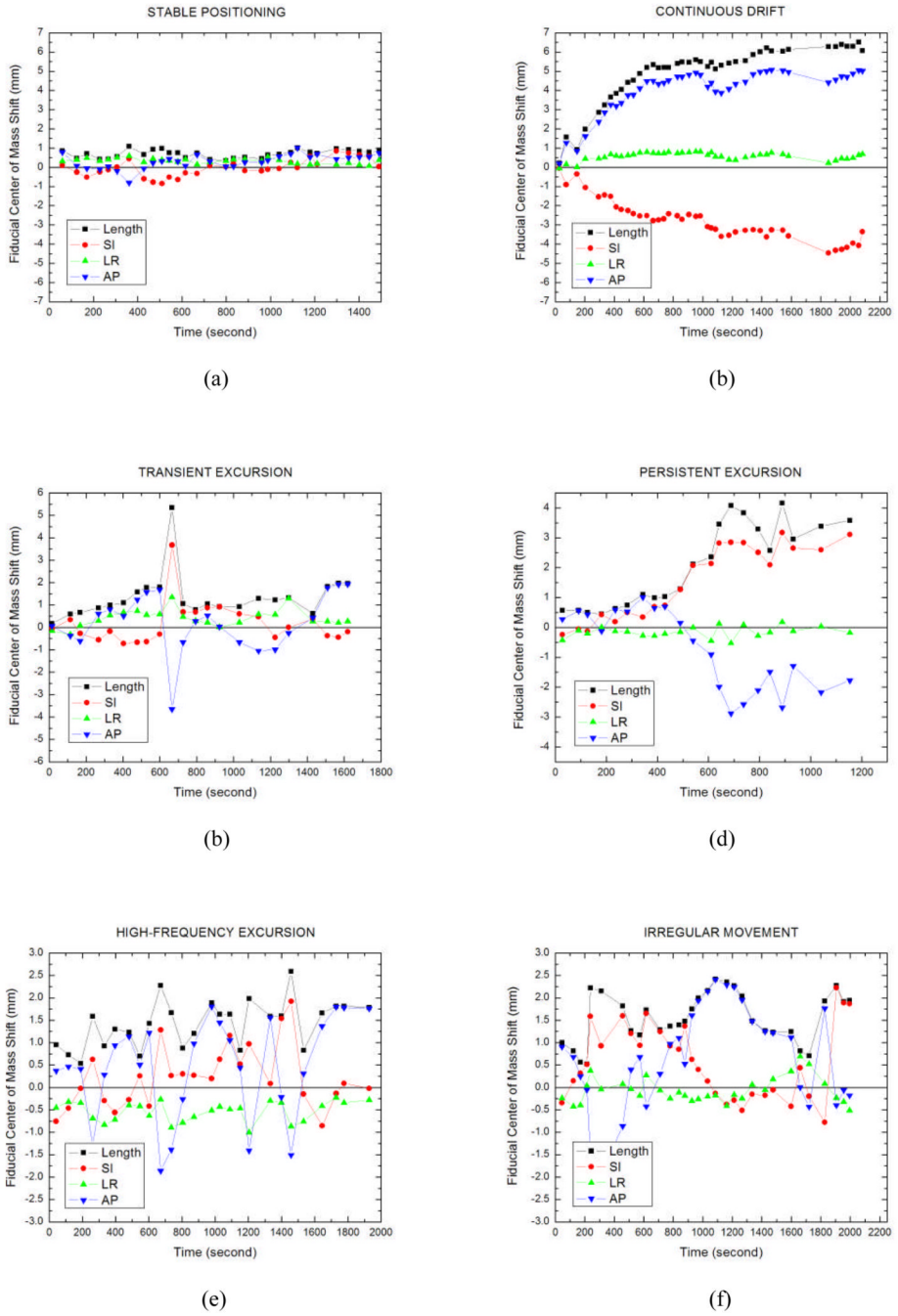

Figure 6.

Patterns of prostate movement: (a) stable target at baseline, (b) continuous drift, (c) transient excursion, (d) persistent excursion, (e) high-frequency excursion, and (f) irregular movement (red: superior/inferior direction; green: left/right direction; blue: anterior/posterior direction; black: vector length of the shift).

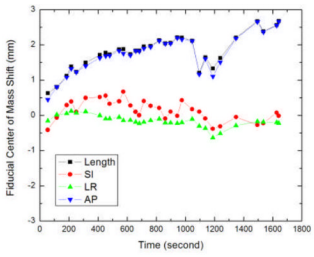

Data set 1

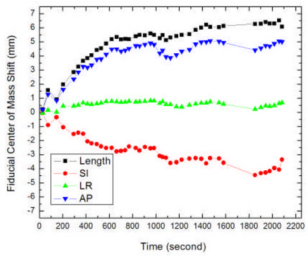

Data set 2

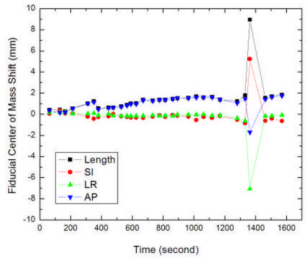

Data set 3

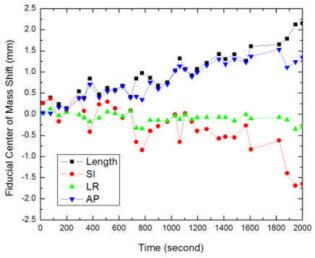

Data set 4

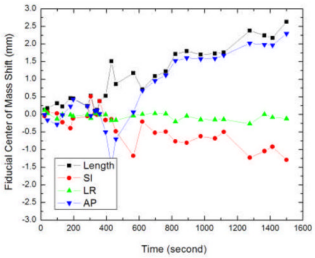

Data set 5

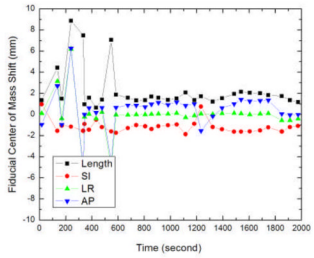

Data set 6

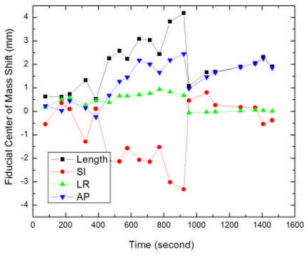

Data set 7

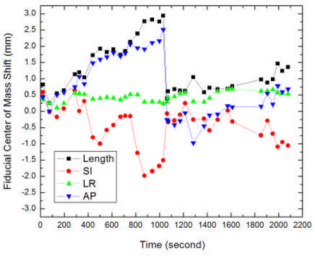

Data set 8

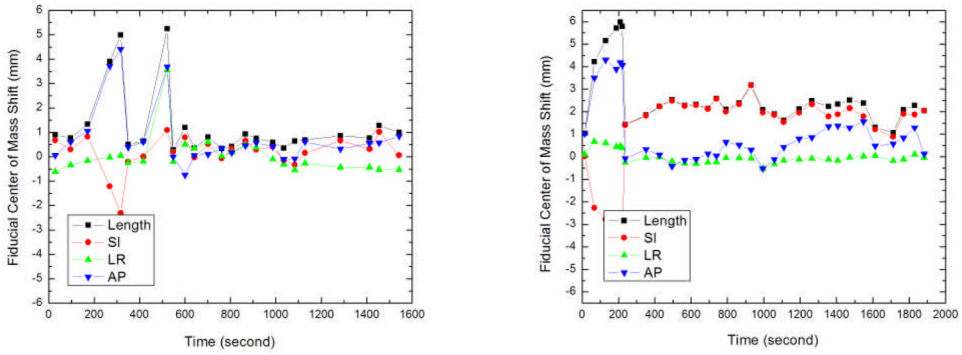

Figure 7.
Prostate movement behaviors for one of the patients in different data sets (red: superior/inferior direction; green: left/right direction; blue: anterior/posterior direction; black: vector length of the shift).

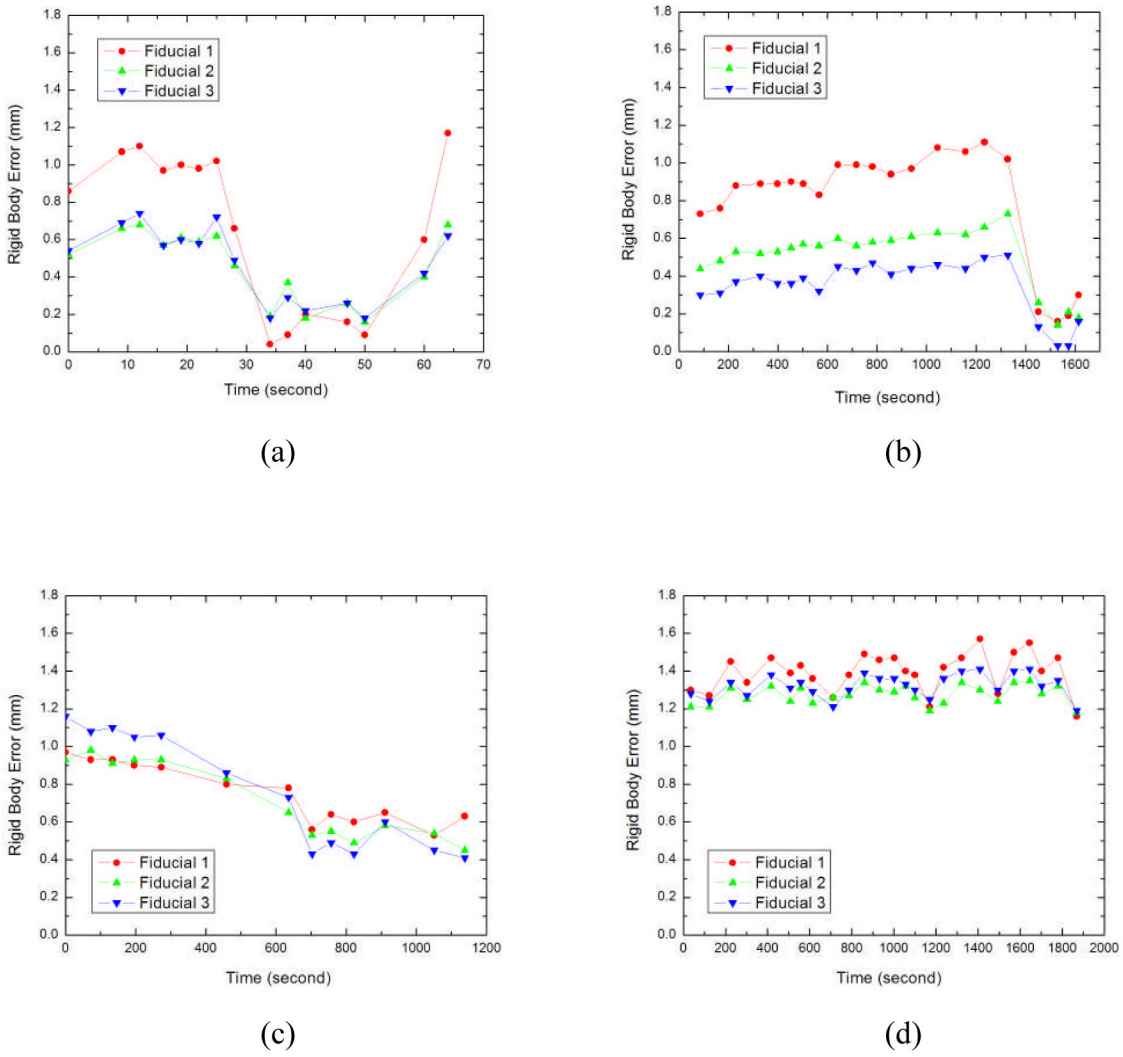

Figure 8.
Rigid Body Error curve of three fiducials for four representative patients (red: Fiducial 1; green: Fiducial 2; blue: Fiducial 3).

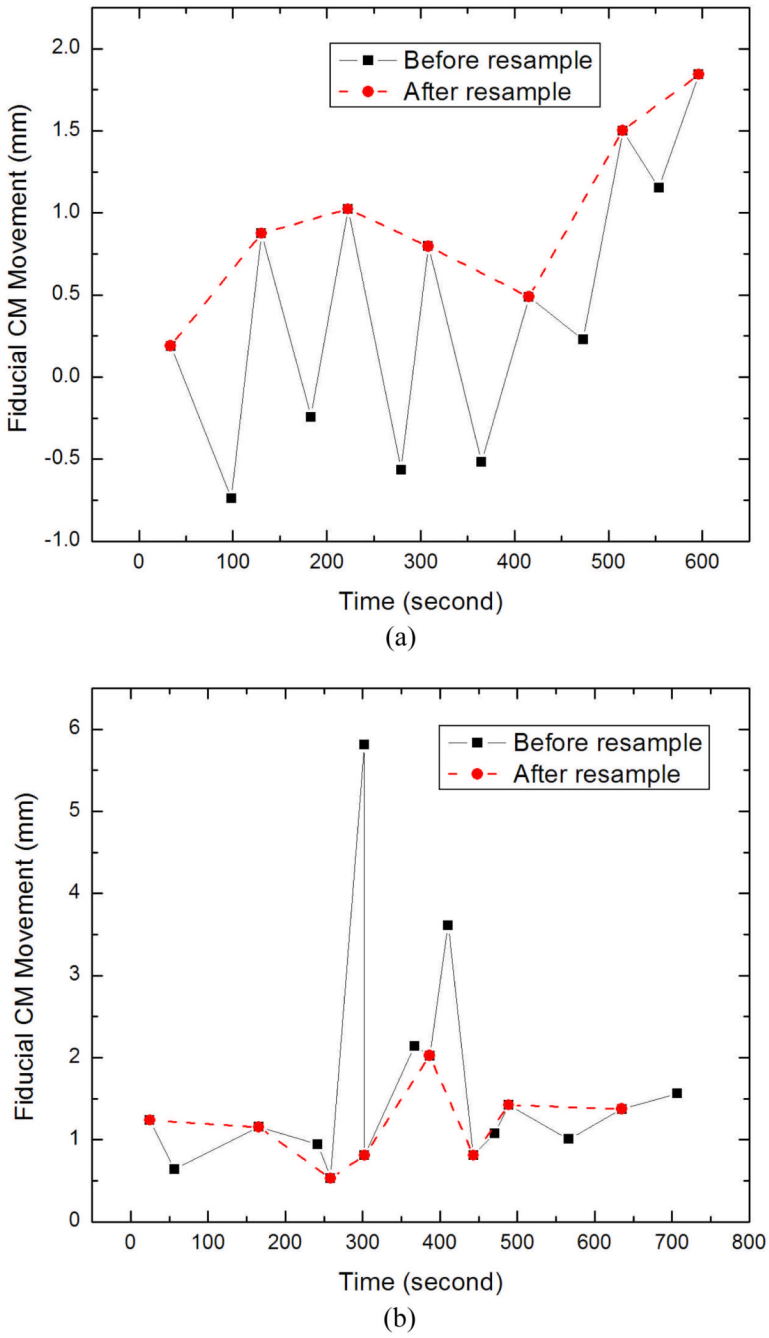

Figure 9.
Prostate movement behaviors depicted by stereoscopic imaging of two different sample rates for two patients. (a) patient 1, (b) patient 2.

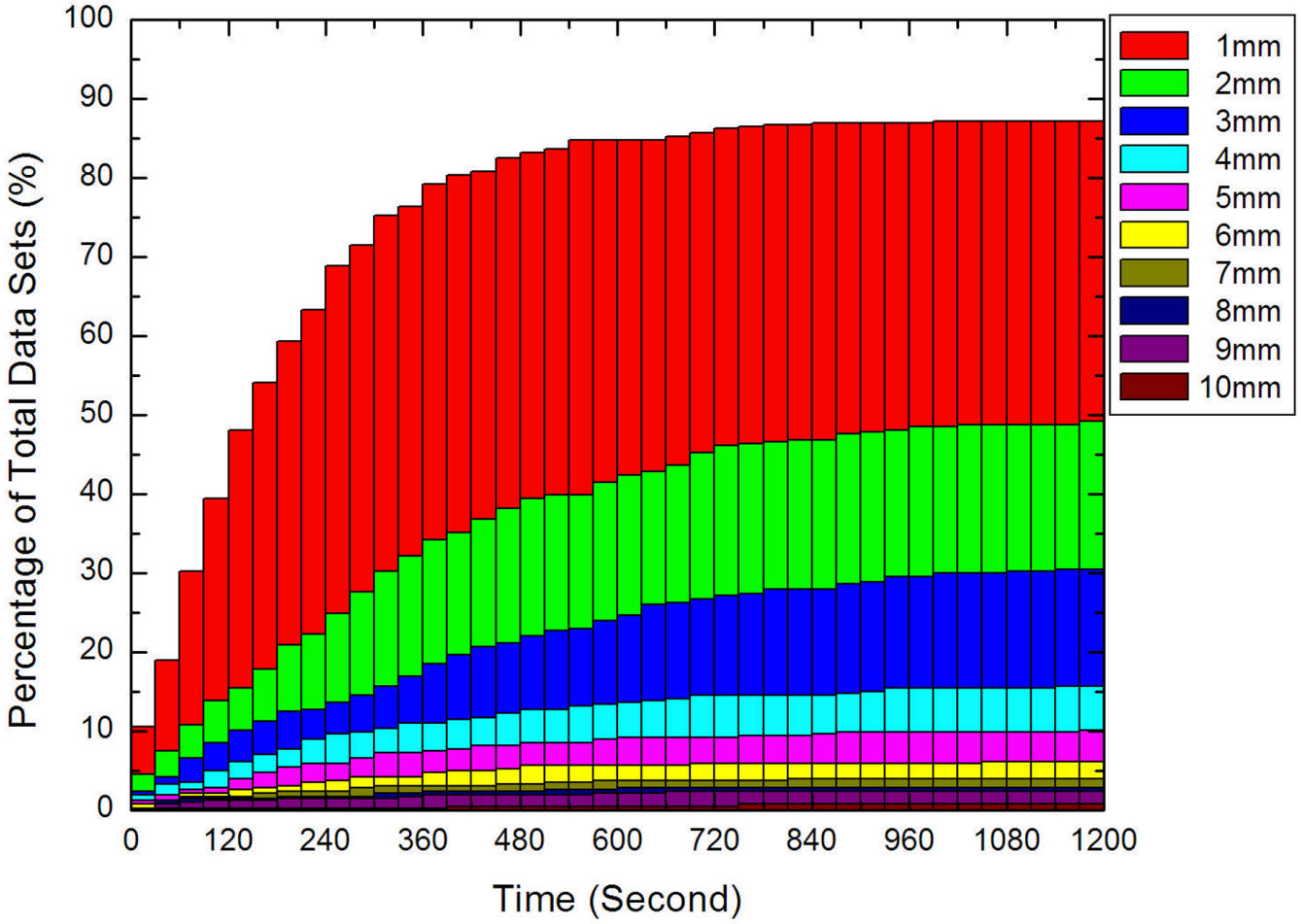

Figure 10.
Percentage of data sets for the prostate target as a function of time duration and movement threshold.

Table 1

Statistical characterization of the 427 data sets for each direction (SI, LR and AP) and the vector length of the shift (Length).

	SI	LR	AP	Length
Average (mm)	1.55	0.87	1.80	2.61
SD (mm)	1.28	1.17	1.44	1.94

Table 2

Correlation coefficients between three fiducials for four representative cases.

	Patient 1	Patient 2	Patient 3	Patient 4
Fiducial 1&2	96.2%	97.7%	94.9%	97.8%
Fiducial 1&3	96.9%	98.2%	98.4%	99.2%
Fiducial 2&3	97.6%	97.0%	98.1%	98.8%

Table 3

Percentage of data sets having movement threshold from 1 mm to 5 mm for a few sampling intervals of interest.

		Prostate Movement Threshold				
		1mm	**2mm**	**3mm**	**4mm**	**5mm**
Sampling Interval	30s	10.5%	4.4%	2.3%	1.9%	1.2%
	60s	19.0%	7.5%	4.2%	3.2%	1.9%
	90s	30.2%	10.8%	6.6%	3.5%	2.6%
	120s	39.3%	13.8%	8.4%	4.9%	2.8%